Temperature Dependent Electrical and Electrocaloric Properties of Textured 0.72PMN - 0.28PT Ceramics*

Irem Bobrek, Ayse Berksoy-Yavuz, M. Yunus Kaya, Sedat Alkoy, M. Baris Okatan, I. Burc Misirlioglu & Ebru Mensur-Alkoy

Taylor & Francis
Taylor & Francis Group

Check for updates

Temperature Dependent Electrical and Electrocaloric Properties of Textured 0.72PMN - 0.28PT Ceramics*

Irem Bobrek[a], Ayse Berksoy-Yavuz[a,b], M. Yunus Kaya[a,c], Sedat Alkoy[a], M. Baris Okatan[d], I. Burc Misirlioglu[e], and Ebru Mensur-Alkoy[a]

[a]Department of Materials Science and Engineering, Gebze Technical University, Kocaeli, Turkey;
[b]Department of Metallurgical and Materials Engineering, Istanbul Gedik University, Istanbul, Turkey;
[c]Department of Metallurgical and Materials Engineering, Bursa Technical University, Bursa, Turkey;
[d]Department of Materials Science and Engineering, Izmir Institute of Technology, Izmir, Turkey;
[e]Faculty of Engineering and Natural Sciences, Sabanci University, Istanbul, Turkey

ABSTRACT

Lead magnesium niobate (PMN) - lead titanate (PT) solid solution ceramics in the ratio of 0.72PMN-0.28PT was produced by a combination of tape-casting in $\langle 001 \rangle_{pc}$ textured and random forms. The Lotgering factor, f, of textured ceramics was approximately calculated as 80%. Modified Curie-Weiss analysis indicated relaxor dominant behavior for both the random and textured ceramics. Development of texture led to an enhancement in the electromechanical properties with converse piezoelectric charge coefficient (d_{33}*) under 20 kV/cm electric field reaching 545 pm/V for the textured ceramic. Electrocaloric (EC) behavior of random and textured ceramics were obtained from indirect measurements using temperature dependent polarization vs. electric field hysteresis loops. An EC temperature change (ΔT_{EC}) of $\sim$0.5 K was calculated from the PMN-28PT ceramics at around 80 °C under an electric field of 60 kV/cm. Development of texture was demonstrated to have led to an anisotropy in the EC response.

1. Introduction

Lead based $(1-x)Pb(Mg_{1/3}Nb_{2/3})O_3–xPbTiO_3$ (PMN-xPT) solid solutions are relaxor ferroelectric materials with perovskite structure. PMN-xPT compositions in single crystal form usually exhibit high dielectric constants and piezoelectric coefficients (d_{33}~ 2500 pC/N), low hysteresis, and a large strain level of $\sim$1.7%. Thus, it is a promising material for sonar transducers, multilayer ceramic capacitors, telecommunication devices, large strain actuators, and other devices [1,2].

The magnitude of properties of PMN-xPT solid solutions depend on the ratio of the end members. The rhombohedral phase region with low titanium (Ti) concentration and tetragonal phase region with high Ti concentration are separated by a Morphotropic Phase Boundary (MPB) in the PMN-PT phase diagram. Highest ferroelectric properties

for the PMN-PT are exhibited in this MPB area due to existence of multiple numbers of polarization states. Despite numerous studies on the complex polar states and the dielectric relaxation behavior, there are still aspects regarding the ferroelectricity of relaxor based ferroelectrics that needs to be investigated. Firstly, different phases are energetically very close to each other particularly in the MPB region, hence, they may either co-exist or may easily transform to each other as a result of external stimuli. Secondly, external conditions may cause structural and chemical disorder in PMN-PT. Finally, the unique polar states of PMN, i.e. the polar nanoregions (PNRs), induce considerably distinct dielectric and piezoelectric properties compared to normal ferroelectrics with macroscopic domains. All the aforementioned critical issues affect the diffuse phase transition in the PMN-PT system. Phase transition behavior is also influenced from the composition, annealing conditions, oxygen partial pressure, applied electric field, pressure, and temperature [2,3].

Due to the superior properties compared to piezoceramics, PMN-PT have been grown in single crystal form using Bridgman method. Although, most of the single crystal growth studies [4] focused on the PMN-32.5PT composition, since it shows the highest piezoelectric properties, there are also few studies in the literature on the PMN-25PT [5] and PMN-10PT [6] compositions, as well. However, PMN-PT single crystals have some limitations in terms of cost, size, and compositional uniformity. Hence, crystallographically textured PMN-PT ceramics that are produced by the combination of tape casting and templated grain growth (TGG) have also been investigated as a cost-effective alternative. TGG process leads to the development of a crystallographic texture in polycrystalline ceramics through the growth of grain-oriented template particles [7]. Textured materials have a single preferred orientation such as (001) in perovskite piezo-electrics, and in PMN-PT, this texture is induced through the use of $BaTiO_3$ or $SrTiO_3$ template particles [8]. As an example, Sabolsky et al.[9] used $BaTiO_3$ template particles to obtain a texture in the $<001>_{pc}$ direction in PMN-32.5PT with a Lotgering Factor of 0.82. These textured samples showed 0.32% strain at 45 kV/cm and a converse piezoelectric coefficient (d_{33}^*) ranging from 1200 pm/V to 1400 pm/V measured under a unipolar electric field (< 10 kV/cm). In another study, Kwon et al. [10] used $SrTiO_3$ template particles to generate $\langle 001 \rangle_{pc}$ texture in PMN-32.5PT and obtained high values of field induced strain (>0.30% at 50 kV/cm) and high d_{33} coefficient (>1600 pC/N at 5 kV/cm) [11]. Comparison of the underwater electroacoustic device performance of PMN-28PT composition in single crystal, crystallographically $\langle 001 \rangle_{pc}$ textured and randomly oriented ceramic form has also been reported by Brosnan et al. [12], where single crystal performed best with the highest source level and largest bandwidth and textured ceramic performed better than the random case.

PMN-PT system has also generated interest for possible electrocaloric applications [13–16]. Electrocaloric effect (ECE) is the adiabatic temperature/entropy change that is observed in a dielectric material as a result of an externally applied electric field, and it is a promising phenomenon for miniaturized solid-state cooling devices [17]. ECE is a first rank tensor property and thus it should display an anisotropy in non-centrosymmetric ferroelectric materials [18]. There are studies in the literature on anisotropy of the ECE in PMN-PT single crystals of various compositions, namely PMN–24PT [19], PMN–25PT [5], PMN–27PT [20], PMN–30PT [15]. However, the anisotropy of ECE in

the crystallographically textured ceramics have only been reported recently by Mensur-Alkoy et al. [16] in the PMN-10PT composition.

In this study, the effect of $\langle 001 \rangle_{pc}$ texture and quenching process on the dielectric, piezoelectric, ferroelectric and electrocaloric properties of the $0.72Pb(Mg_{1/3}Nb_{2/3})O_3-0.28PbTiO_3$ (PMN-28PT) composition was investigated and discussed. This composition is on the rhombohedral side of the MPB at room temperature and located at the vicinity of the invariant point of the ferroelectric phases with rhombohedral and tetragonal symmetries and the paraelectric phase with cubic symmetry in the PMN-PT phase diagram [21]. It was selected due to the multiple numbers of polarization states, which would decrease the anisotropy energy, leading to an easier switching between various polarization states, and thus an enhanced EC response and promising soft piezoelectric properties for sensor applications.

2. Experimental

Conventional solid state calcination method was used to synthesize the composition of $0.72Pb(Mg_{1/3}Nb_{2/3})O_3-0.28PbTiO_3$ (PMN-28PT) ceramic powders. A two-step processes was used to obtain the PMN-0.28PT composition, where columbite method was initially used to synthesize magnesium niobate ($MgNb_2O_6$) from magnesium carbonate hydroxide pentahydrate $(MgCO_3)_4 \cdot Mg(OH)_2 \cdot 5H_2O$ (Sigma Aldrich, 98%) and niobium pentoxide (Nb_2O_5) (Alfa Aesar, 99.5%) source powders. In the second step, lead carbonate $((PbCO_3)_2 \cdot Pb(OH)_2)$ (Sigma Aldrich), titanium oxide (TiO_2) (Degussa, P25) were mixed with the magnesium niobate ($MgNb_2O_6$) powders obtained in the first step in stoichiometric ratios and ball-milled with in ZrO_2 media in ethanol and dried at $70\,°C$ on hotplate. Then green powders were calcined at $850\,°C$ for $4\,h$ with $2\,wt\%$ lead oxide excess.

The plate-like $BaTiO_3$ (BT) template particles were synthesized with the combination of molten salt synthesis (MSS) and topochemical microcrystal conversion (TMC) methods [22,23]. Samples were fabricated by tape-casting method and the slurries for this casting process were prepared from the calcined PMN-0.28PT powders using an organic binder mixture and ethanol + MEK as solvent. Grain oriented PMN-28PT samples were prepared with $5\,vol\%$ BT templates. The tapes were casted using doctor blade with $200\,\mu m$ blade gap with the casting speed of $10\,cm/s$ on a glass substrate. The green tapes were removed from the glass substrate after $2\,h$ drying. The tapes were punched and then laminated at $80\,°C$ under uniaxial pressure at $100\,MPa$. The green samples were then pressed with cold isostatic press (CIP) at $150\,MPa$. Finally, organic content was removed from the green ceramics at $600\,°C$ for $1\,h$ with a heating rate of $1\,°C/min$, followed by sintering at $1150\,°C$ for $4\,h$ in an oxygen rich atmosphere. The final thicknesses of the ceramics were adjusted as $500\,\mu m$ and $1000\,\mu m$.

The phase analysis of the powders and ceramics were done using X-ray diffractometer (XRD) (Bruker D8 Advanced, Germany) with a Cu-K$_\alpha$ radiation in the $2\theta = 20°-60°$ range with a step size of $0.02°$. Indexing of the diffraction peaks were done assuming a pseudo-cubic symmetry. The degree of grain orientation along $\langle 001 \rangle_{pc}$ in the textured ceramics was calculated from XRD patterns using the Lotgering's method [24]. The surface and cross-sectional microstructure of the ceramics was examined by scanning electron microscope (SEM) (Philips XL30 FEI Co., USA). The samples were prepared for

the SEM investigation by grinding and polishing, followed by thermal annealing for 30 min at 980 °C. The polarization versus electric field hysteresis loops (P-E) of samples were measured with a period of 2000 ms using a Precision LC ferroelectric tester (Radiant Technologies, Inc., USA) and these measurements were conducted from 90 °C down to 0 °C during the cooling cycle. Bipolar and unipolar strain (x-E) behaviors of the ceramics were measured with a MTI 2000 photonic sensor (MTI Instrument Inc., USA) at room temperature. The temperature dependence of dielectric constant (ε_r) and loss tangent (tanδ) of samples were measured at 1–100 kHz using LCR meter (Hioki 3520, Hioki, Japan) from room temperature (RT) up to 250 °C by heating at 2 °C/min. Piezoelectric charge constant, d_{33}, were measured by Berlincourt method. Piezoelectric voltage constant, g_{33}, of the samples were calculated using measured dielectric permittivity and d_{33} of the samples. Electrocaloric response of the PMN–28PT ceramics was determined by indirect method [25] through measurements of the electrical polarization P(T,E) as a function of the temperature and the electric field E while cooling from 90 °C down to 0 °C.

3. Results and Discussion

The PMN-PT powder was prepared by solid-state calcination method and from the XRD analysis the powder exhibited pure perovskite phase (not shown here). Particle size distribution of the powder was measured by particle size analyzer. SEM micrograph and particle size distribution of the powders were given in Fig. 1. Narrow and submicron particle size distribution was obtained, and mean particle size was found to be 0.17 μm.

The XRD analyses of random (R) and textured (T) ceramics were given in Fig. 2. These two ceramics were crystallized in perovskite phase without any secondary phases. It was seen from Fig. 2 that the random ceramic had the highest intensity for $(110)_{pc}$ peak, as expected from the perovskite structure, while the intensities of the $(110)_{pc}$ and other (hkl) peaks of textured ceramics decreased with the development of texture. The
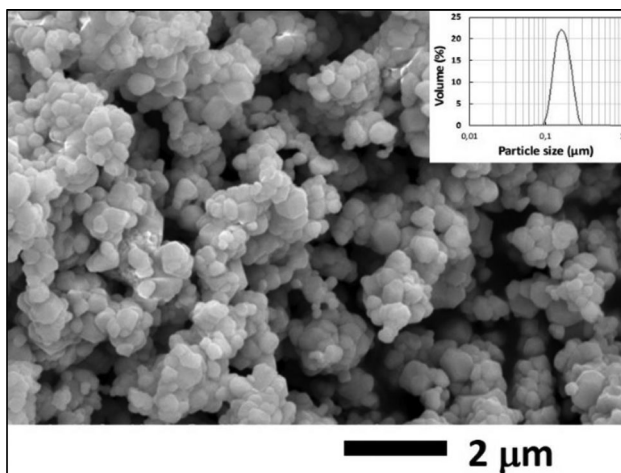
Figure 1. SEM micrograph and (inset) particle size distribution of 0.72PMN-0.28PT powder.
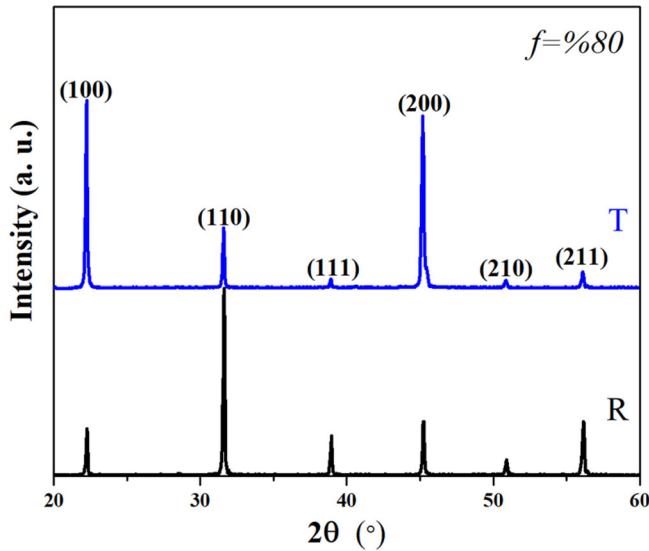
Figure 2. Comparison of the XRD patterns of textured (T) and random (R) ceramic samples.

intensities of (00l) peaks increased sharply in the textured ceramics. The Lotgering factor, f, of textured ceramics was approximately calculated as 80% for this system. In order to evaluate the symmetry of the random and textured ceramics, the (111) and (002) peaks of both random and textured ceramics have been investigated in detail by slow XRD scans with finer steps. Peak splitting is expected in the (111) peak in the case of rhombohedral symmetry, which is expected to be the case for the compositions with PbTiO$_3$ content lower than the morphotropic phase boundary composition. Splitting in the (002) peak is expected in the case of tetragonal structure, which might be observed if the BT template particles stabilize a tetragonal symmetry. Detailed scans did not reveal any splitting in either case. This is believed to be due to the close proximity of the composition of interest to the morphotropic phase boundary composition, where the structural symmetry is expected to be pseudo-cubic [26].

The cross-sectional SEM micrographs of polished and thermally etched surfaces of randomly oriented and textured ceramics are given in Fig. 3. Both ceramics were found to be fairly dense. The density measurements by the Archimedes' technique indicated densities exceeding 97% of the theoretical value for both random and textured samples. From the SEM micrograph of textured sample given in Fig. 3b, it is clearly seen that the edge-on template particles (thin slab-like regions embedded in the grains with dark contrast) were aligned fairly uniformly through the matrix and parallel to the tape casting direction, which was the horizontal direction in this case. The preferred texture development was successfully obtained in the $\langle 001 \rangle_{pc}$ direction.

The comparison of the dielectric constants (ε_r) and loss tangent (tan δ) of the random and textured samples with respect to temperature measured at the frequencies of 1 kHz, 10 kHz and 100 kHz are shown in Fig. 4. Both samples exhibited a sharp transition from ferroelectric phase to paraelectric phase at the Curie temperature (T$_c$) of 132 °C and 126 °C for random and textured samples at 1 kHz, respectively. The textured ceramic had a lower maximum dielectric constant ($\varepsilon_{rmax} \sim$21,594 at 1 kHz) compared to
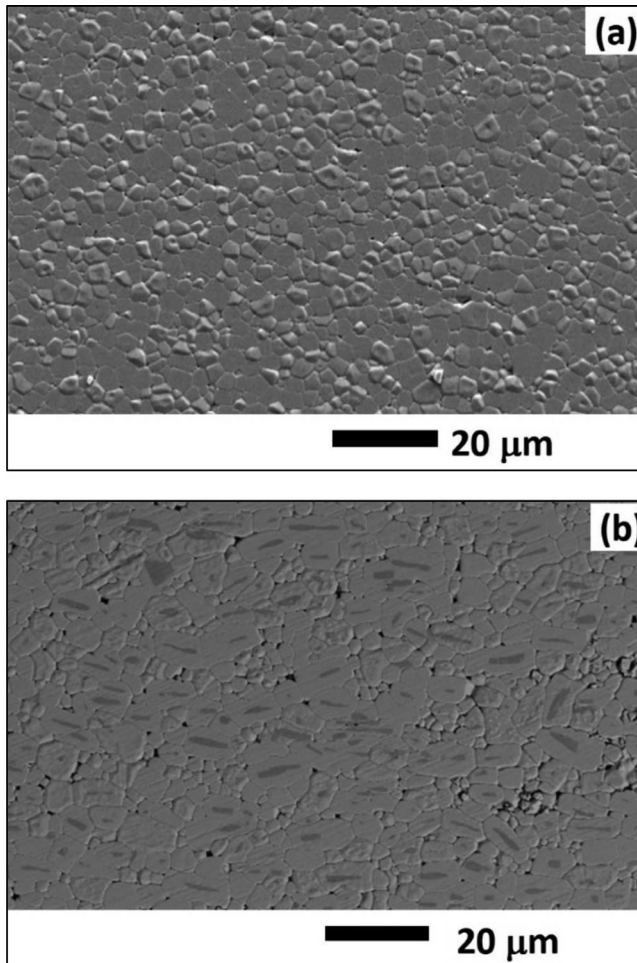
Figure 3. SEM micrographs of (a) random and (b) textured ceramics.

the random ceramics ($\varepsilon_{rmax} \sim 28,000$ at 1 kHz). This could be attributed to the elastoelectric composite effect owing to using BT templates (5 vol% ratio) with low ε_r [1,8]. A similar trend of decreasing peak value of textured ceramics has also been seen in the literature [16,27–29] and has been discussed in detail in a previous report [16]. From Fig. 4, the measurement frequency was also found to cause a slight shift in the peak value of the dielectric constant at T_m, which was attributed to the relaxor behavior of this composition. Moreover, a broadening of the peaks was observed for textured samples.

In regular and commensurate ferroelectrics, the temperature dependence of the dielectric constant above the dielectric constant maximum can be described with the Curie-Weiss law [30]. However, as it is clearly seen from Fig. 4, both the random and textured ceramics with the PMN-0.28PT composition displayed relaxor-like characteristics as demonstrated by the diffuseness of the phase transition, frequency dependence of the dielectric constant maximum, and thus, a strong deviation from the Curie-Weiss behavior at high temperatures is expected [31]. This deviation can be described with a modified relationship [30–33] as it is given in the following equation:
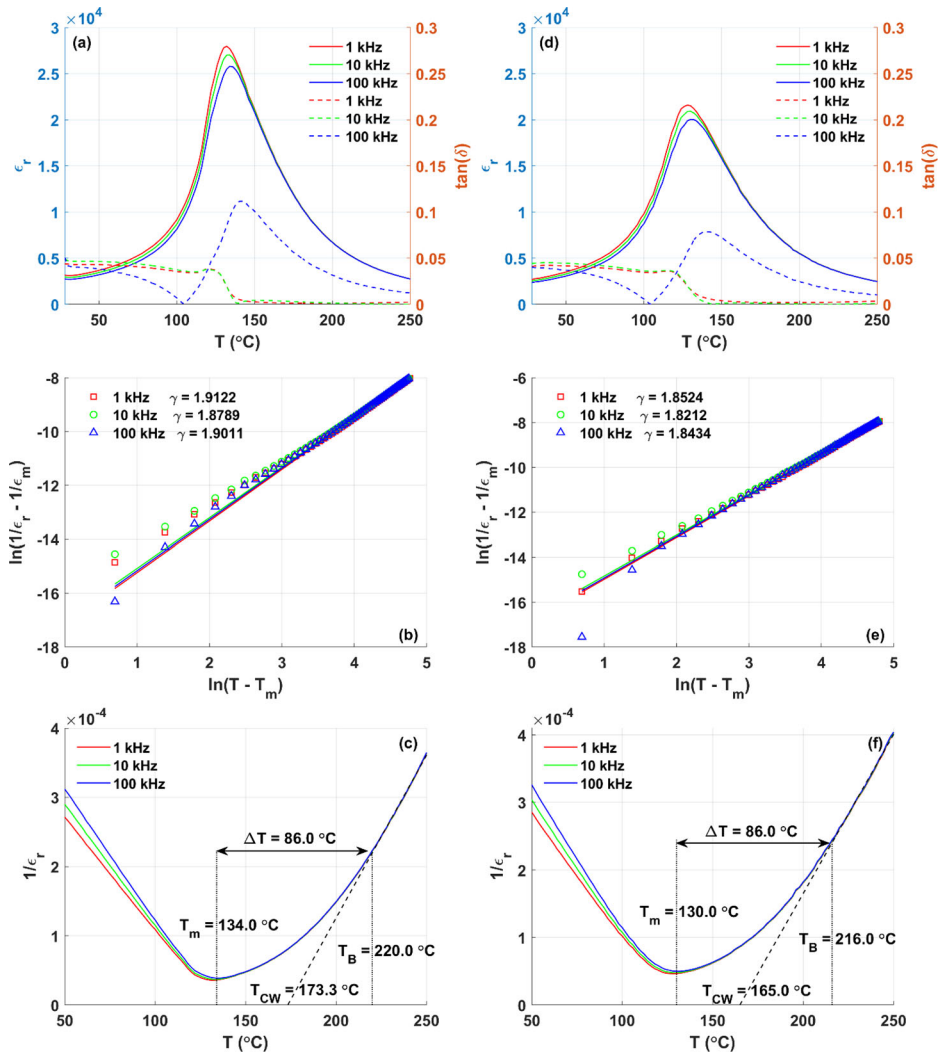
Figure 4. Temperature dependence of dielectric constant and dielectric loss of (a) random and (d) textured ceramics. Log-log plots of and temperature dependence of the inverse permittivity of (b) and (c) random, and (e) and (f) textured ceramics measured at various frequencies.

$$\frac{1}{\varepsilon_r} - \frac{1}{\varepsilon_m} = \frac{(T - T_m)^{\gamma}}{C} \tag{1}$$

where ε_m is the peak value of the dielectric constant, the T_m is the temperature at which maximum dielectric constant is observed, C is the Curie constant, and γ is the degree of broadening or diffusiveness of the phase transition. The γ ranges from 1 in normal ferroelectrics to 2 in relaxor ferroelectrics. The temperature dependent dielectric behavior of the PMN-28PT ceramics in the current study were investigated to identify and evaluate the deviation from the Curie-Weiss law. The γ parameter was determined by linear curve fitting to data represented in log-log plots, as given in Fig. 4b and e. The γ value was calculated as 1.90 for the random and 1.84 for the textured ceramic at 100 kHz. These values indicate a relaxor dominant character for both ceramics and agrees with
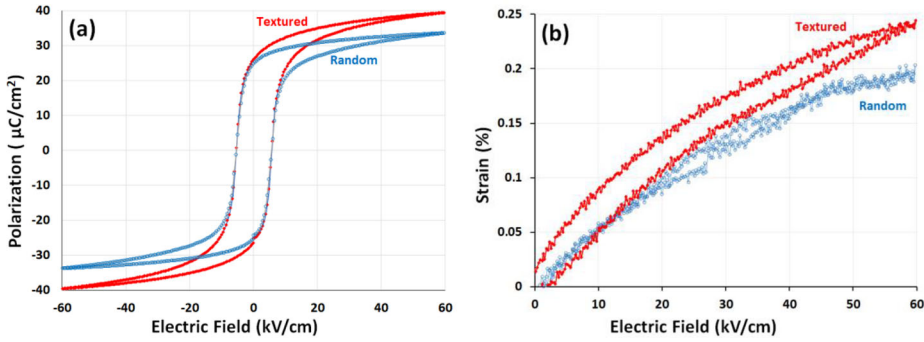
Figure 5. Electric field induced (a) polarization hysteresis loops and (b) strain curves of random and textured ceramics.

the literature [26]. It was also found that presence of BT templates with a normal ferro-electric behavior or the crystallographic texture did not lead to a critical change in the characteristics of the PMN-28PT ceramics. The deviation from the Curie-Weiss law was also confirmed with the temperature dependent inverse permittivity plots given in Fig. 4c and f for the random and textured ceramics, respectively. The dashed lines in the fig-ures are included to demonstrate the deviation from the Curie-Weiss behavior at high temperatures. Deviation starts at the T_B which was identified with a fine vertical dashed line in the figures. The T_B of the random ceramics was determined as 220 °C, whereas the T_B of the textured ceramics was determined 216 °C, respectively. These results also confirm the relaxor dominant behavior of both the random and textured ceramics.

Polarization vs. electric field (P-E) hysteresis loops of the random and textured cer-amics measured at 0.5 Hz and under 60 kV/cm are shown in Fig. 5a. As seen from this figure, the P-E loop of the random ceramic had a well-saturated, square-like characteris-tic, which is believed to be due to the easier switching of domains, whereas the P-E loop was more slanted in the textured case. This change of character in the textured ceramics indicated that domain wall motion became more difficult, which could be attributed to the clamping effect that arises from the barium titanate templates due to the existence of increasing interfacial stresses.

The electric field induced unipolar strain curves of the PMN-28PT ceramics were measured at room temperature with a triangular waveform at 0.5 Hz frequency and under 60 kV/cm as seen in Fig. 5b. The level of the strain response increased by >20% with texturing. The strain level measured at 60 kV/cm of random sample was deter-mined as 0.19% and it was increased to 0.24% after texturing as seen in Fig. 5b and Table 1. These values indicated that texturing of the samples was rather effective on improving the electromechanical properties. While the piezoelectric charge coefficient, d_{33}, of random ceramic was measured as ∼340 pC/N by Berlincourt method, this value was measured as ∼390 pC/N for textured ceramic. The variation of all dielectric, ferro-electric and electromechanical properties of random and textured ceramics were given in Table I.

Temperature dependent hysteresis behavior of the random PMN-28PT ceramics were also investigated from room temperature up to 90 °C under 60 kV/cm electric field for further investigations of the electrocaloric response and the results of these

Table 1. Electrical properties of random and textured ceramics.

Sample	Random	Texture
T_c (°C) @1 kHz	132	128
ε_r (@30 °C - @1 kHz)	2708	2429
$\varepsilon_{r\text{-max}}$ (@T_c - @1 kHz)	27972	21594
tanδ (@30 °C - @1 kHz)	0.041	0.039
d_{33} (pC/N)	340	390
d_{33}^* (pm/V)(0-20 kV/cm)	475	545
d_{33}^* (pm/V)(@ 60 kV/cm)	325	400
S (%) (Unipolar) @60kV	0.19	0.24
P_r (μC/cm^2) @60kV, @0.5 Hz	24.8	26.5
P_{max} (μC/cm^2) @60kV, @0.5 Hz	33.7	39.4
E_c (kV/cm) @60kV, @0.5 Hz	3.5	3.5
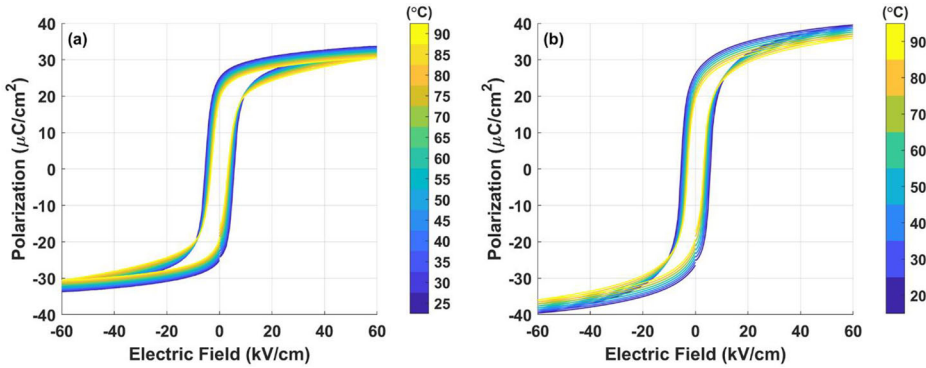
Figure 6. Electric field induced polarization graphs of (a) random and (b) textured PMN–28PT ceramics measured at different temperatures.

measurements were given in Fig. 6a and b for the random and textured PMN-28PT ceramics, respectively. The magnitude of the electrocaloric (EC) response, i.e. the adiabatic temperature change - ΔT_{EC}, and the isothermal entropy change - ΔS, of the PMN-28PT ceramics were calculated from the temperature dependent P-E measurements given in Fig. 6, using the Maxwell relationship of $(\partial P/\partial T)_E = (\partial S/\partial E)_T$. The following equations were used in these computations [25]:

$$\Delta S = -\int_{E_1}^{E_2} \left(\frac{\partial P}{\partial T}\right)_E dE \tag{2}$$

$$\Delta T_{ec} = -\int_{E_1}^{E_2} \frac{T}{C\rho}\left(\frac{\partial P}{\partial T}\right)_E dE \tag{3}$$

where ρ, C and $(\partial P/\partial T)_E$ are the heat capacity, density and the pyroelectric coefficient of the material under a change of electric field, respectively. The pyroelectric coefficient was determined from the positive upper branch of the P vs E hysteresis loops (Fig 6b). The derivative of P vs T data at constant E, i.e. the pyroelectric coefficient, was calculated in two different ways: **(i)** from 4th order polynomial fits and **(ii)** from finite differences on a linear interpolator.

Pyroelectric coefficients, ΔS vs T_o and ΔT vs T_o plots for the random and $\langle 001 \rangle_{pc}$ textured PMN–28PT ceramics were given in Fig. 7a–7c and d–f, respectively. From these figures the maximum ΔT_{EC} determined indirectly from the temperature
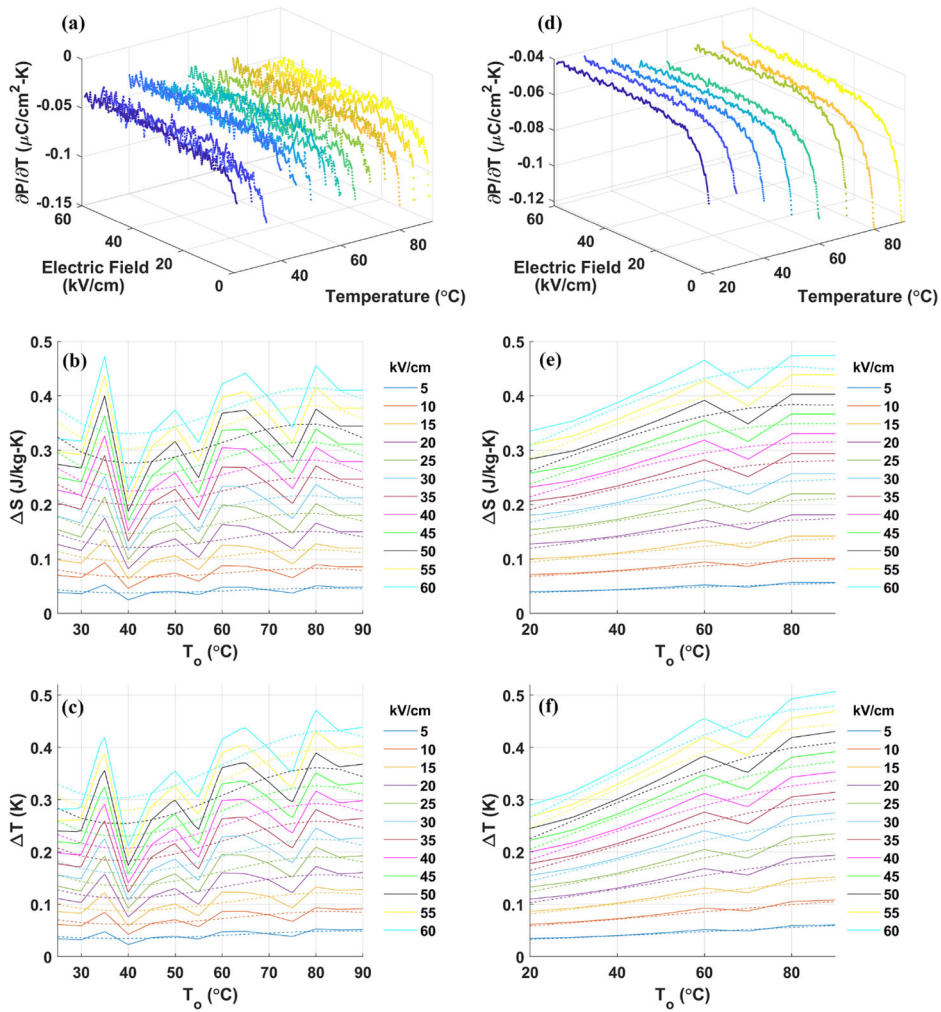
Figure 7. (a) and (d) Pyroelectric coefficient, (b) and (e) ΔS vs T_o and (c) and (f) ΔT vs T_o plots of (a)–(c) random and (d)–(f) $\langle 001 \rangle$pc textured PMN–28PT ceramics. In (c), (d) and (e), (f) solid and dashed lines represent, at several electric field strengths, E_2 and ($E_1 = 0$ kV/cm), respectively, results based on use of pyroelectric coefficient determined via interpolation and fourth order polynomial fits.

dependent P-E measurements within the range of measurement temperatures were found to be around 0.5 K under 60 kV/cm electric field. These values are similar to the results reported by Rozic et al. [34] in a similar temperature regime under 60 kV/cm for a PMN-30PT composition, which is very close to the composition investigated in our study. The ΔT_{EC} values obtained from the textured ceramics was slightly (~10%) higher compared to the random case. The ΔT_{EC} values are expected to be higher close to the phase transition temperature, which is around 130 °C in the current case and it was beyond the upper limit of our measurement setup. Additionally, in the perovskite relaxor ferroelectric materials, the ΔT_{EC} was reported to reach its highest values of 2–3 K under electric field amplitudes ranging from 60 to 90 kV/cm, which were the amplitudes for an electric-field-induced ferroelectric phase transition [34]. Due to the

lower breakdown fields of the samples in our samples, field levels beyond 60 kV/cm have not been tried.

Although, a limited enhancement was observed with the development of texture, the crystallographic orientation of the grains and the applied field direction, both of which were along the $\langle 001 \rangle_{pc}$ direction, was unfavorable due to the inherent spontaneous polarization direction of composition of interest. Although, PMN-28PT is at the vicinity of the MPB, it is still on the rhombohedral side of the boundary and in a composition with rhombohedral symmetry, the spontaneous polarization would be along the $\langle 111 \rangle_{pc}$ directions [18]. Thus, $P_{r\langle 001 \rangle}$ is expected to be misoriented from the P_s with an angle of 54.7° and scales up to $1/\sqrt{3}$ of the P_s in textured ceramics, whereas the angles between the P_r values of various grains and the P_s vary from 0° to 54.7° in the case of random ceramics. Thus, the observed polarization values in a $\langle 001 \rangle_{pc}$ textured ceramic would be expected to be lower compared to a $\langle 111 \rangle_{pc}$ textured case when the base symmetry is rhombohedral. This might also reflect positively on the ECE response of the textured
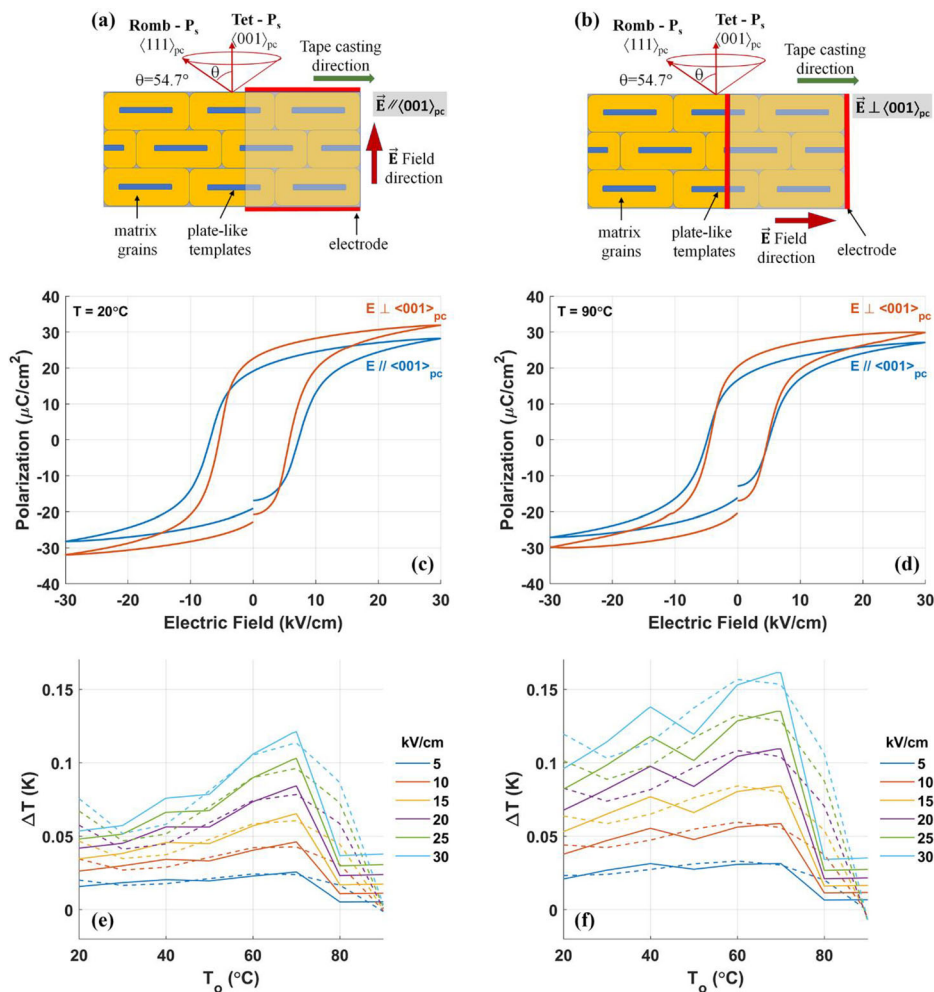
Figure 8. Textured PMN-28PT samples cut parallel and perpendicular to $\langle 001 \rangle_{pc}$ directions.

ceramic. Investigation of the anisotropy of ECE in single crystals in the PMN-PT system with rhombohedral symmetry, such as 0.75PMN–0.25PT [5] and 0.76PMN–0.24PT [19] indicated that crystals cut along the $\langle 111 \rangle_{pc}$ directions displayed a relatively higher electrocaloric performance over the crystals cut along $\langle 110 \rangle_{pc}$ and $\langle 100 \rangle_{pc}$ directions. In the case of textured PMN-28PT ceramics in our study, there is a clear crystallographic orientation of grains along the $\langle 001 \rangle_{pc}$ direction, however, the $\langle 111 \rangle_{pc}$ directions of these grains are oriented along a cone of equal possibility, as shown in Fig. 8a and b. Nevertheless, an electric field applied along a direction perpendicular to the crystallographic texture direction, i.e. E $\perp$ $\langle 001 \rangle_{pc}$ should be expected to induce a more favorable orientation of the P_r with P_s since a direction parallel to $\langle 001 \rangle_{pc}$ would have an angle of 35.3° with the P_s, which is along the $\langle 111 \rangle_{pc}$ direction. In order to investigate the validity of this axiom thicker (t ≈ 3 mm) samples were prepared from the textured ceramics. Although, the field handling of the thicker textured samples was lower than the thinner ones due to possible densification issues, the results were informative in themselves. As a reference of standard, samples were cut from the thick ceramic piece and electroded in the usual way, as shown in Fig. 8a, which was identified as E // $\langle 001 \rangle_{pc}$. In the second set of samples, called the E $\perp$ $\langle 001 \rangle_{pc}$, electrodes were coated parallel to the texture direction and thus, electric field was applied perpendicular to the crystallographic texture direction, as shown in Fig. 8b. A clear difference, i.e. anisotropy was observed in the P-E hysteresis loops where the P_r and P_{max} values of the E $\perp$ $\langle 001 \rangle_{pc}$ samples were higher compared to the E // $\langle 001 \rangle_{pc}$, as shown in Fig. 8c and d for measurements taken at 20 °C and 90 °C, respectively. This difference was found to reflect positively on the EC response of the E $\perp$ $\langle 001 \rangle_{pc}$ case where slightly higher ΔT_{EC} values were observed. These results indicated that texturing PMN-PT ceramics with rhombohedral symmetry along $\langle 111 \rangle_{pc}$ direction should further enhance the electrocaloric response.

4. Conclusion

Temperature dependent dielectric, ferroelectric and electrocaloric properties of $\langle 001 \rangle_{pc}$ textured PMN-28PT ceramics ($f_{001} \sim 80\%$) obtained by TGG process using a 5 vol% of BaTiO$_3$ template particles have been investigated. This composition was specifically chosen due to its proximity to the morphotropic phase boundary in the PMN-28PT. A relaxor dominant behavior for both the random and textured ceramics were observed from dielectric constant vs. temperature measurements and this was further confirmed by a modified Curie-Weiss analysis. While texture development led to a decrease in the dielectric properties due to the clamping effect of the BT templates, the ferroelectric and electromechanical properties were found to increase. Although, crystallographic texture along $\langle 001 \rangle_{pc}$ direction did improve the electrocaloric response of the PMN-28PT ceramics, the texture direction was not found to be entirely favorable, and that a texture along $\langle 111 \rangle_{pc}$ would be expected to yield a better electrocaloric response due to the $\langle 111 \rangle_{pc}$ orientation of the spontaneous polarization direction in the composition with rhombohedral symmetry.

Funding

References

1. X. Lu *et al.*, Temperature-dependent phase transition in [001] C-oriented 0.72Pb(Mg$_{1/3}$Nb$_{2/3}$)O$_3$ - 0.28PbTiO$_3$ single crystals, *Ceram. Int.* **45** (11), 13999 (2019). DOI: 10.1016/j.ceramint.2019.04.099.

2. H. Sabarou *et al.*, Structural investigation of oxygen stoichiometry during thermocycles in PMN-28PT, *J. Alloys Compd.* **784**, 592 (2019). DOI: 10.1016/j.jallcom.2018.12.358.

3. F. Li *et al.*, Local structural heterogeneity and electromechanical responses of ferroelectrics: Learning from relaxor ferroelectrics, *Adv. Funct. Mater.* **28** (37), 1801504 (2018). DOI: 10.1002/adfm.201801504.

4. S. E. Park and T. R. Shrout, Ultrahigh strain and piezoelectric behavior in relaxor based ferroelectric single crystals, *J. Appl. Phys.* **82** (4), 1804 (1997). DOI: 10.1063/1.365983.

5. G. Sebald *et al.*, Electrocaloric and pyroelectric properties of 0.75Pb(Mg$_{1/3}$Nb$_{2/3}$)O$_3$–0.25PbTiO$_3$ single crystal, *J. Appl. Phys.* **100** (12), 124112 (2006). DOI: 10.1063/1.2407271.

6. L. Luo *et al.*, Pyroelectric and electrocaloric effect of <111>-oriented 0.9PMN–0.1PT single crystal, *J. Alloys Compd.* **509** (32), 8149 (2011). DOI: 10.1016/j.jallcom.2011.05.111.

7. K. H. Brosnan *et al.*, Templated grain growth of < 001> textured PMN-28PT using SrTiO$_3$ templates, *J. Amer. Ceram. Soc.* **92**, S133 (2009). DOI: 10.1111/j.1551-2916.2008.02628.x.

8. S. Gollapudi *et al.*, Electric field induced splitting of the preferred orientation in PMN-PT textured ceramics, *J. Am. Ceram. Soc.* **102** (9), 5038 (2019). DOI: 10.1111/jace.16462.

9. E. M. Sabolsky, S. Trolier-McKinstry, and G. L. Messing, Dielectric and piezoelectric properties of <001> fiber-textured 0.675Pb(Mg$_{1/3}$Nb$_{2/3}$)O$_3$– 0.325PbTiO$_3$ ceramics, *J. Appl. Phys.* **93** (7), 4072 (2003). DOI: 10.1063/1.1554488.

10. S. Kwon *et al.*, ⟨001⟩ Textured 0.675Pb(Mg$_{1/3}$Nb$_{2/3}$)O$_3$-0.325PbTiO$_3$ ceramics: templated grain growth and piezoelectric properties, *J. Am. Ceram. Soc.* **88** (2), 312 (2005). DOI: 10.1111/j.1551-2916.2005.00057.x.

11. K. H. Brosnan *et al.*, Texture Measurements in < 001> Fiber-Oriented PMN–PT, *J. Am. Ceram. Soc.* **89** (6), 1965 (2006). DOI: 10.1111/j.1551-2916.2006.01049.x.

12. K. H. Brosnan *et al.*, Comparison of the properties of tonpilz transducers fabricated with < 001> fiber-textured lead magnesium niobate-lead titanate ceramic and single crystals, *J. Acoust. Soc. Am.* **126** (5), 2257 (2009). DOI: 10.1121/1.3238158.

13. J. Peräntie *et al.*, Electrocaloric properties in relaxor ferroelectric $(1 - x)$Pb(Mg$_{1/3}$Nb$_{2/3}$)O$_3$–xPbTiO$_3$ system, *J. Appl. Phys.* **114** (17), 174105 (2013). DOI: 10.1063/1.4829012.

14. U. Plaznik *et al.*, Bulk relaxor ferroelectric ceramics as a working body for an electrocaloric cooling device, *Appl. Phys. Lett.* **106** (4), 043903 (2015). DOI: 10.1063/1.4907258.

15. J. Li *et al.*, Complex phase transitions and associated electrocaloric effects in different oriented PMN-30PT single crystals under multi-fields of electric field and temperature, *Acta Mater.* **182**, 250 (2020). DOI: 10.1016/j.actamat.2019.11.017.

16. E. Mensur-Alkoy *et al.*, Effect of texture on the electrical and electrocaloric properties of 0.90Pb(Mg$_{1/3}$Nb$_{2/3}$)O$_3$–0.10PbTiO$_3$ relaxor ceramics, *J. Appl. Phys.* **128** (8), 084102 (2020). DOI: 10.1063/5.0003296.

17. S. P. Alpay *et al.*, Next-generation electrocaloric and pyroelectric materials for solid-state electrothermal energy interconversion, *MRS Bull.* **39** (12), 1099 (2014). DOI: 10.1557/mrs.2014.256.

18. R. E. Newnham, *Properties of Materials: Anisotropy Symmetry, Structure* (Oxford University Press, New York, 2005), pp. 58–71.

19. T. F. Zhang et al., Orientation related electrocaloric effect and dielectric phase transitions of relaxor PMN-PT single crystals, *Ceram. Int.* **43** (18), 16300 (2017). DOI: 10.1016/j.ceramint.2017.08.217.

20. B. Lu et al., Enhanced electrocaloric effect in $0.73Pb(Mg_{1/3}Nb_{2/3})O_3-0.27PbTiO_3$ single crystals via direct measurement, *Crystals* **10** (6), 451 (2020). DOI: 10.3390/cryst10060451.

21. Z.-G. Ye et al., Monoclinic phase in the relaxor-based piezoelectric/ferroelectric $Pb(Mg_{1/3}Nb_{2/3})O_3-PbTiO_3$ system, *Phys. Rev. B.* **64** (18), 184114 (2001). DOI: 10.1103/PhysRevB.64.184114.

22. D. Liu, Y. Yan, and H. Zhou, Synthesis of Micron-Scale Platelet $BaTiO_3$, *J. Am. Ceram. Soc.* **90** (4), 1323 (2007). DOI: 10.1111/j.1551-2916.2007.01525.x.

23. A. Berksoy-Yavuz et al., Structural and electrical properties of (001) textured 0.26PIN-0.40PMN-0.34PT ternary system, *J. Mater. Sci: Mater. Electron.* **30** (20), 18548 (2019). DOI: 10.1007/s10854-019-02208-w.

24. F. K. Lotgering, Topotactical reactions with ferrimagnetic oxides having hexagonal crystal structures-I, *J. Inorg. Nucl. Chem.* **9** (2), 113 (1959). DOI: 10.1016/0022-1902(59)80070-1.

25. Z. Kutnjak, and B. Rožič, Indirect and direct measurements of the electrocaloric effect, in *Electrocaloric Materials: New Generation of Coolers*, edited by Tatiana Correia and Qi Zhang (Springer, Heidelberg; Berlin, 2014), pp.125–146.

26. R. Yimnirun, Dielectric properties of lead magnesium niobate – lead titanate ceramics prepared by mixed oxide method, *Int. J. Mod. Phys. B.* **23** (03), 403 (2009). DOI: 10.1142/S0217979209049760.

27. G. L. Messing et al., Templated grain growth of textured piezoelectric ceramics, *Crit. Rev. Solid State Mater. Sci.* **29** (2), 45 (2004). DOI: 10.1080/10408430490490905.

28. T. Richter et al., Textured PMN–PT and PMN–PZT, *J. Am. Ceram. Soc.* **91** (3), 929 (2008). DOI: 10.1111/j.1551-2916.2007.02216.x.

29. A. Berksoy-Yavuz, and E. Mensur-Alkoy, Electrical properties and impedance spectroscopy of crystallographically textured $0.675[Pb(Mg_{1/3}Nb_{2/3})O_3]$ - $0.325[PbTiO_3]$ ceramics, *J. Mater. Sci: Mater. Electron.* **29** (15), 13310 (2018). DOI: 10.1007/s10854-018-9455-8.

30. K. Uchino, and S. Nomura, Critical exponents of the dielectric constants in diffused-phase-transition crystals, *Ferroelectrics* **44** (1), 55 (1982). DOI: 10.1080/00150198208260644.

31. X. Dai, Z. Xu, and D. Viehland, The spontaneous relaxor to normal ferroelectric transformation in La-modified lead zirconate titanate, *Philos. Mag. B* **70** (1), 33 (1994). DOI: 10.1080/01418639408240192.

32. M. Y. Kaya et al., Influence of compositional variation on the electrical properties of $[Pb(Zn_{1/3}Nb_{2/3})O_3]$-$[Pb(Zr,Ti)O_3]$ ceramics and their transducer application, *IEEE Trans. Ultrason. Ferroelectr. Freq. Control* **65** (7), 1268 (2018). DOI: 10.1109/TUFFC.2018.2829800.

33. O. Cakmak et al., Investigation of the electrical properties of textured $0.5[Ba(Zr_{0.2}Ti_{0.8})]O_3$-$0.5[(Ba_{0.7}Ca_{0.3})TiO_3]$ piezoceramics, *J. Mater. Sci: Mater. Electron.* **31** (5), 4184 (2020). DOI: 10.1007/s10854-020-02971-1.

34. B. Rožič et al., Influence of the critical point on the electrocaloric response of relaxor ferroelectrics, *J. Appl. Phys.* **110** (6), 064118 (2011). DOI: 10.1063/1.3641975.